

A Comparative Study of the Diagenesis in Diapir-Influenced Reef Atolls and a Fault Block Reef Platform in the Late Albian of the Vasco-Cantabrian Basin (Northern Spain)

J. REITNER¹

1 Introduction

The Mesozoic Vasco-Cantabrian Basin is situated in the Spanish Basque-Lands of northern Spain, close to the French border (Fig. 1). To the west the basin is delineated by the Paleozoic massifs of the Cantabrian Mountains, to the east by the Pyrenees, and to the south by the Late Tertiary Ebro Basin. The tectonic history of the Vasco-Cantabrian ranges from the Triassic to the Tertiary but the major part of its fill (8000 m) is attributed to Late Mesozoic deposition. During the Late Albian due to rapid subsidence, salt diapirs (Keuper age) developed between basement fault blocks. Shallow marine carbonate reefs (Urgonian Facies) developed on these highs. Two types of reef can be distinguished: (1) larger fault block reef platforms on tilted basement segments and (2) smaller reef atolls on top of rising diapirs. The diapir reefs can be differentiated from the fault block reefs through sedimentological, paleobiological, diagenetic, and geochemical criteria.

The purpose of this paper is to present the different diagenetic phases in diapir reefs and fault block reef development. To achieve this, the respective paleobiological and sedimentological frameworks will be described first and the petrographic and geochemical aspects of the diagenetic sequences will be treated subsequently.

2 Previous Studies

The first detailed work on the "Keuper" diapirs of northern Spain by Lotze (1953) did not include facies analysis. Brinkmann et al. (1967) studied some of these diapirs in greater detail using facies and structure analysis. Von Stackelberg (1967) first suggested that the small-sized carbonate reefs of the Late Campanian Oro Limestone situated above the Murguía diapir may have been indirectly linked to the diapir. Other similar smaller carbonate reefs also exist near the Villasana de Mena diapir of the Vasco-Cantabrian Basin. These latter reefs are especially interesting since the presence of large quantities of reworked Keuper material indicates a collapse event in the Villasana de Mena diapir during the Late Albian (Vraconian) (Schroeder 1980, Schroeder and Willems 1983, Reitner

¹ Institut für Paleontologie, Freie Universität, Schwendener Straße 8, 1000 Berlin 33, FRGermany

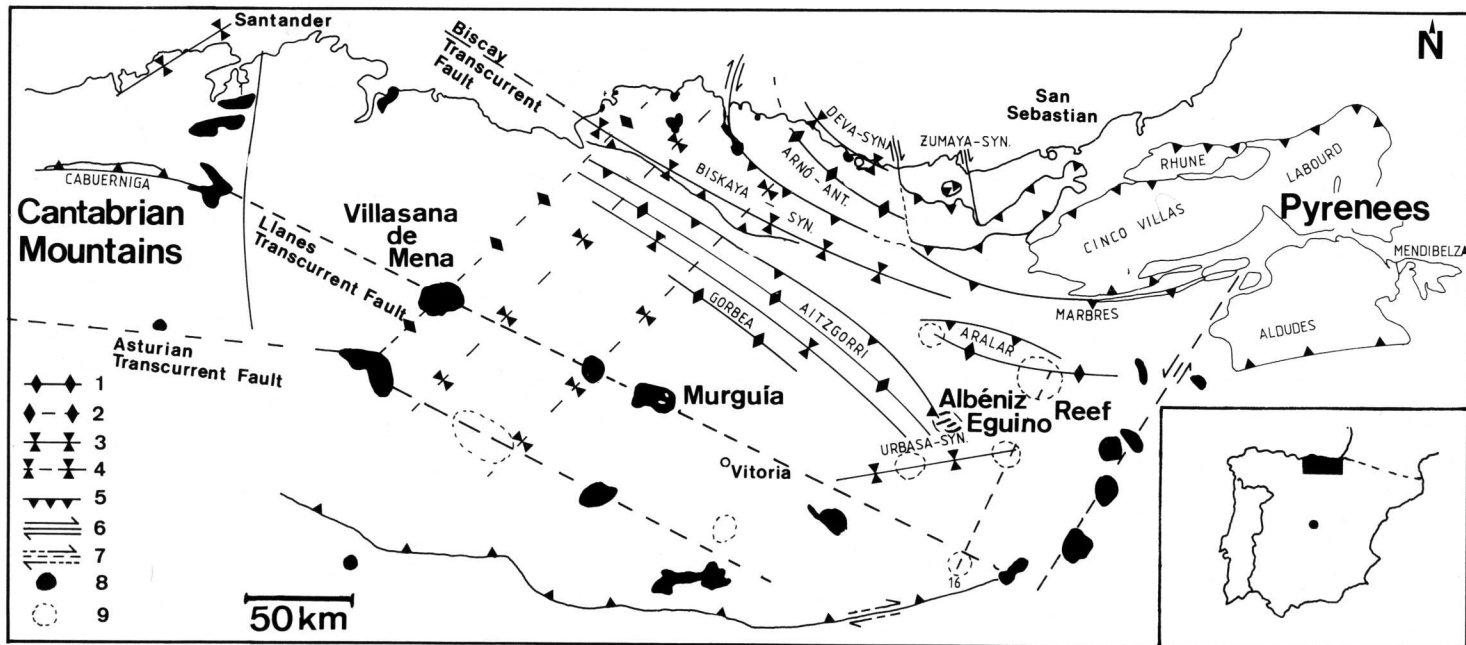


Fig. 1. Location map and geological structure of the Vasco-Cantabrian Basin in northern Spain (Reitner 1985). 1 Anticline; 2 assumed anticline; 3 syncline; 4 assumed syncline; 5 thrust fault; 6 strike slip fault; 7 assumed strike slip fault; 8 salt diapirs; 9 salt pillows

1980, 1982). According to Reitner (1985), this may also be the case in the Murguía diapir. This presentation deals with the carbonate reefs associated with these two diapirs.

3 Methods

The Villasana de Mena diapir and the Murguía diapir were mapped in detail. Sections across each diapir were measured and the lithological changes were established according to biologic, sedimentologic, and petrographic criteria. A similar procedure was followed in the fault block constituting the Albeníz-Eguino reef platform of the same area.

Diagenetic features were studied by petrographic microscope, scanning electron microscope (SEM) with energy dispersive X-ray analyzer, atomic absorption spectrometry (AAS), and X-ray fluorescence. Selected thin sections were stained with potassium ferricyanide in order to distinguish between Fe and Fe-free calcites.

4 Diapir Reef Atolls

4.1 The Late Albian Villasana de Mena Reef Atoll (Caniego Limestone)

4.1.1 Reef Structure

Due to outcrop conditions, the original reef structure cannot be determined with precision. The size of the reef, however, may correspond to the diameter of the diapir roof which may have measured 2 to 5 km. Sedimentation in the surrounding basins consisted of prodelta muds (Blank 1983). The ascending diapir formed a submarine dome which lifted the diapir roof out of the terrigenous influence into the photic zone and allowed the development of a reef. In an advanced stage, the diapir roof collapsed due to salt subsidence. In this process the reef carbonates were fractured and dissected by fissures and crevices through which diapiric material, such as Keuper pelites, hypersaline brines, and Keuper ophites, were extruded. A small diapir basin may have developed within the reef with a surrounding barrier of grainstone shoals and coralgall framework. With this atoll-like structure, water circulation between the open sea and the diapir lagoon was probably restricted.

4.1.2 Facies Belts of the Caniego Limestone (Fig. 2)

There are five distinctive facies belts within the Caniego Limestone, but only the key facies for diapir reef identification are summarized here. A more detailed profile, which includes 16 facies zones, is presented in Reitner (1985). The facies belts, ranging from the basin and slope to lagoonal, have sharp contacts.

The basin and slope facies belt is distinguished by reef debris and planktonic foraminifera while the reef core belt contains the corallgal framework. The reef flat belt is characterized by rudists and grainstone shoals while the lagoonal facies contains a hypersaline fauna (miliolid foraminifera and thin-shelled ostracods) and tempestites. The intertidal facies belt resembles the typical Loferite mudstone facies of the Late Triassic Dachstein Limestone of the Northern Calcareous Alps (Fischer 1964).

4.2 The Late Albian Murguía Diapir

Another example of an Albian diapir reef system is found 50 km east of the Villasana de Mena diapir. The Murguía diapir exhibits further facies and diagenetic peculiarities as a result of the influence of salt brines. The first major feature of the Murguía diapir is the ooid facies which was aragonitic. This is in sharp contrast to other Cretaceous ooid facies which were exclusively calcitic (Sandberg 1975, 1983). The Mg/Ca ratios in the Cretaceous open sea was 2:1, while in the area of the diapirs the Mg/Ca ratio may have reached 5:1 due to the Mg-rich salt brines. This may have promoted the production of aragonitic ooids in the diapir reef lagoon (Lippmann 1973) (Fig. 7e, f).

The second major feature of the Murguía diapir is the presence of sulfide ores in the fractures and fissures of the reef. The circulation of diapiric waters through the reef complex caused the formation of sphalerite, galena, pyrite, etc. (Lietz 1951) (Fig. 8d). The Vasco-Cantabrian Basin contains a large resource potential in sulfides and sulphates.

5 Fault Block Reef Platform

5.1 The Late Albian Albeniz-Eguino Reef Platform (Figs. 1 and 3)

This reef platform is situated about 70 km east of the Villasana de Mena diapir and is about 150 square km in area. The reef beds range from 200 to 500 m in thickness and consist of eight separate reef bodies, each separated by deep grabens filled by siliciclastic pelites and carbonate turbidites. The Albeniz-Eguino reef platform is situated on tilted fault blocks (the Aitzgorri high), this type of reef platform being a typical shelf-margin island platform. The sedimentary cycles comprising the platform carbonates are transgressive. They range in age from the uppermost Middle Albian to the lower Late Albian (*Rotalipora ticinensis* zone) (Reitner 1985).

Five facies belts are distinguished in this reef platform. The basin and slope facies belt contains common planktonic foraminifera and debris flows of reef material containing coralline sponges while the reef core facies belt is composed of a corallgal framework and the reef flat facies has caprinid rudists. The carbonate intertidal facies belt contains mudcracks and stromatolites. The hypersaline lagoon facies is characterized by miliolid foraminifera while the littoral intertidal facies consists of siliciclastics.

Facies belts

Tide



Basin/slope

Reef core

Reef flat

*Caprina/
Plagloptychus belt*

Grainstone shoal

Sequences of Diagenesis

**Major
Lithology
Fauna
Flora**

Wackestones: Packstones Planktonic foram Planktonic crinoids Cephalopods	Framestones Floatstones Microsolenid-coral Coralline algae Coralline sponges	Wacke-, Float-, Packstones Caprinid rudists Rhodoliths of coralline algae Orbitolinid forams	Cross-bedded grainstones, rudstones Trocholinid forams
--	--	---	---

Marine phreatic

Reworking of reef sediments
Stromatolitic hardgrounds with phosphorites
Partial replacement of the phosphates by pyrite
Partial reworking of the stromatolitic crusts

Micrite envelopes

Micrite envelopes, coated grains

Marine vadose

Beachrock; meniscus and dripstone cements

Fresh water vadose

Dissolution of aragonite

Dissolution of biogenics
Red micrite filling
Dog tooth II-dripstones

Aragonite dissolution; molds
Dog tooth II dripstones
Vadose slit
Reworking; lithoclasts
Micrite fill

Time

Marine phreatic

Radiaxial fibrous calcitic cement

Marine vadose

Fresh water phreatic

Neomorphic calcite
Bladed ferroan calcite

Red micrite filling; calcitic dog tooth III-cements
Equant calcite cement

Syntaxial calcitic overgrowth

Syntaxial calcitic overgrowth
Equant calcite

Fresh water vadose

Fresh water phreatic

Deep burial

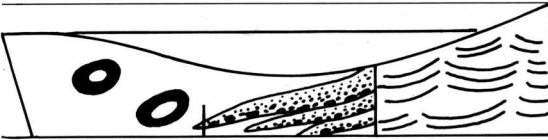
Partial dolomitization of cements

Stylolites
Bitumen

Stylolites
Bitumen

Stylolites
Bitumen

Bitumen



	Lagoon	Mudstone belt	Intertidal
<i>Polyconites/ Toucasia belt</i>			
Wackestones	Mudstones	Mudstones	Mudstones
Floatstones	Wackestones	Wackestones	Wackestones
Requienid rudists	Packstones	Packstones	Bindstones (Stomatolites)
Carpotinid rudists	Ostracods	Ostracods	Ostracods
Miliolid forams			
		Stromatactis Sulphates, proto- dolomites Replacement of sulfates by quartz Micrite fill	Storm layers
			Fibrous dripstone- cement
Dissolution of aragonite Dog tooth II- dripstone Vadose silts	Microkarst		Sheet cracks, tepees Intraformational breccia
Fibrous isopachus cement			
		Dog tooth I-drip- stone in stroma- tactis	
Dog tooth III- calcite cement	Equant ferroan calcite	Equant ferroan calcite cement	
Brecciation Rotation of components Fissures			
Micrite fill Dog tooth III-cement Equant ferroan calcite cement			
	Replacement of ferroan calcite by dolomite Calcedony Pyrite Gypsum cements Sulfur cements	Dolomite/ankerite Authigenic quartz cement	
Stylolites Bitumen	Stylolites Bitumen	Stylolites Bitumen	

Fig. 2. Facies model and diagenetic environments of the Villasana de Mena diapir reef platform (Caniego Limestone)

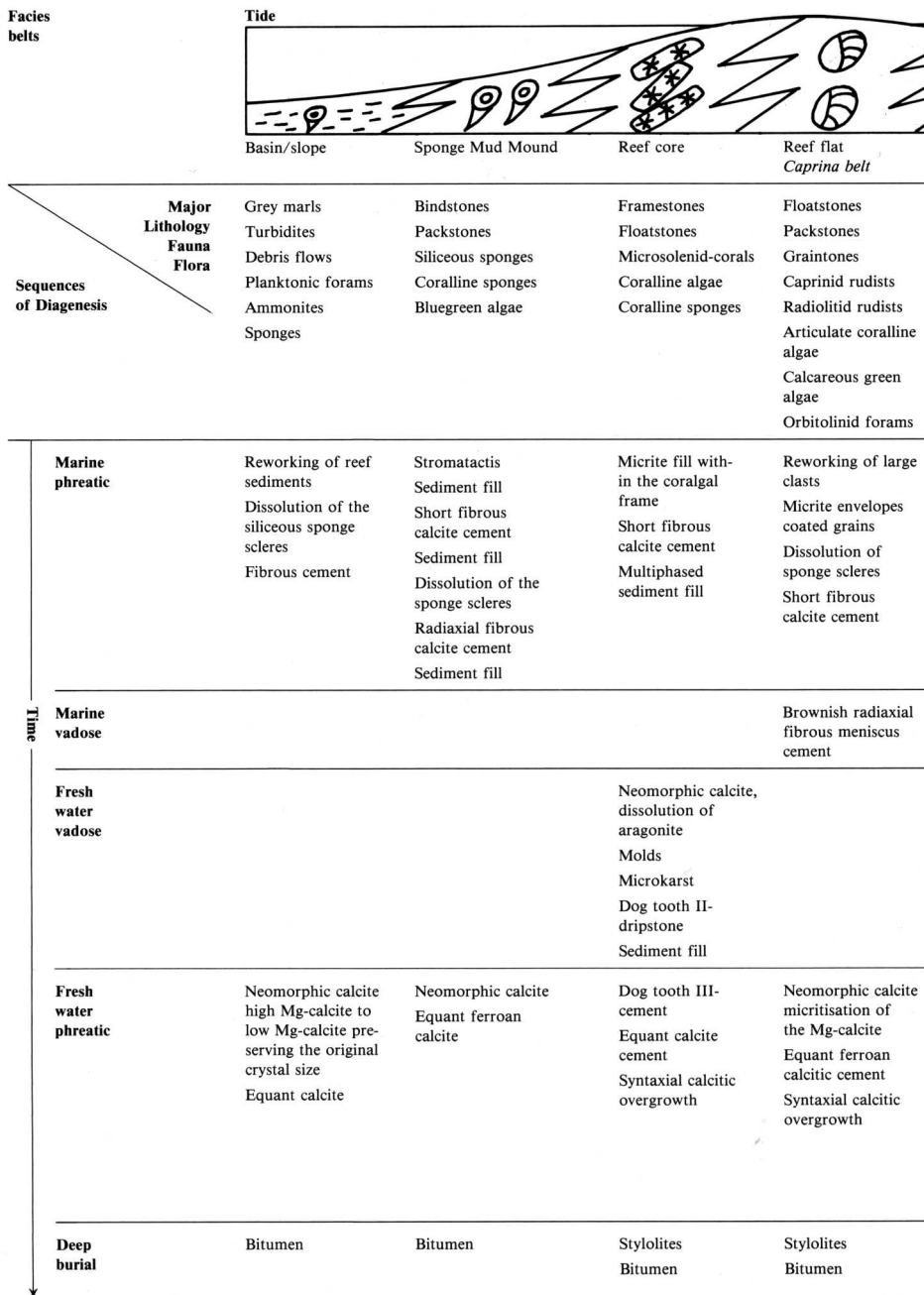


Fig. 3. Facies model and diagenetic environments of the Albeniz-Eguino fault block reef platform



Reef flat Grainstone belt	Intertidal mud-pank	Lagoon	Siliciclastic littoral
Grainstones Rudstones Trocholinid forams Coralline algae	Mudstones Wackestones Bindstones (Stromatolites) Ostracods	Well bedded wacke- stones, mudstones Miliolid and arenaceous forams	Well sorted medium and fine grained beach and inter- tidal sandstones
Reworking of clasts Micrite envelopes coated grains Short fibrous calcite cement	Short fibrous isopachous cement Shrinkage Brownish radial fibrous calcitic cement	Glauconite in forams Reworking of clasts with micrite envelopes	Lithoclasts Micrite envelopes
	Dog tooth I- dripstone calcite cement		
	Dissolution of aragonite Molds		Dissolution of Bio- genics Molds
Neomorphic calcite Dog tooth III- cement Equant ferroan calcite Syntaxial calcitic overgrowth	Dog tooth III- calcitic cement Equant ferroan calcite cement	Neomorphic calcite molds Dog tooth III- calcitic cements Chert replaced calcite Equant ferroan calcite cement	Dog tooth III- calcite cement Intergranular granular calcite cement Limonic cement relacing the calcitic granular cement Syntaxial calcitic overgrowth
Stylolites Bitumen	Bitumen	Pyrite	Sparry dolomites replacing the granular cements

Table 1. Characteristics and interpretations of observed cements

Cement	Fig.	Composition	Habit/fabric	Dimensions	Interpretation	Reference
Bladed scalenohedral type I	4a	Neomorphic low-Mg calcite	Dripstone with relic structures of a fibrous cement	40–80 μm	Marine vadose aragonite cement	Purser (1969) Hanor (1978)
type II	4b	Low-Mg calcite	Dripstone without inclusions	50–60 μm	Freshwater vadose cement	Schneider (1977)
type III	4e, 7a, b	Low-Mg calcite	Isopachous crusts	80–330 μm	Freshwater phreatic cement	Pierson and Shinn (1985)
Radiaxial fibrous cement	4d, 5d, 6b	Neomorphic low-Mg calcite	Dripstone, meniscus, multiphased isopachous crusts	20 μm –5 mm	Marine phreatic-marine vadose aragonite cements	Bechstaedt (1974)
Short fibrous calcite cement		Neomorphic low-Mg calcite (~2% MgCO_3 , EDAX)	Isopachous crusts	60–100 μm	Marine phreatic high-Mg calcite cement	Longman (1980)
Micro-granular calcite cement		Neomorphic low-Mg calcite (~1.5% MgCO_3 , EDAX)	Isopachous crusts	15–30 μm	Marine phreatic high-Mg calcite cement	Longman (1980)
Micritic cement		Neomorphic low-Mg calcite (~4–5% MgCO_3 , EDAX)	Dripstone	8–10 μm	Marine vadose high-Mg calcite cement	
Fibrous calcite cement	5b	Neomorphic low-Mg calcite	Tannish colored isopachous crust	80–100 μm	Marine phreatic aragonite or high-Mg calcite cement	
Equant calcite cement	4c	Low-Mg calcite	Blocky crystals with enfacial junctions	100 μm	Freshwater vadose cement	Longman (1980)
Equant ferroan calcite cement	5d	Fe calcite	Blocky crystals with enfacial junctions	100 μm	Freshwater phreatic cement (shallow burial)	Oldershaw and Scoffin (1967)

Bladed cements		Low-Mg calcite	Bladed crystals	100 – 120 μm length 30 – 45 μm width	Meteoric cement	Longman (1980)
Syntaxial cements		Low-Mg calcite	Syntaxial overgrowth on echinoderm and inoceramid skeletal remains	200 – 500 μm	Freshwater phreatic cement	Neugebauer and Ruhrmann (1978)
Sulfate cements	7d	Gypsum, anhydrite	Limpid idiomorphic elongated crystals	50 – 800 μm	Burial cement	
Sulfur cements	8a, b, c	Elementary sulfur	Blocky crystals	100 – 530 μm	Burial cement	Feely and Kulp (1957) Ellison (1971)
Sparry dolomite	7c	Dolomite with Fe-rich zones (X-ray analysis)	Idiomorphic crystals replacing earlier cements	120 – 300 μm	Burial	Mattes and Mountjoy (1980)
Anhedral dolomite		Dolomite	Dolomicrite with brown coloured anhedral crystals	4 – 10 μm	Intertidal, early diagenetic formation	Fischer (1964) Folk and Land (1975)
Ankerite cement		Ankerite (X-ray analysis)	Idiomorphic crystals	100 – 350 μm	Deep burial cement	Oldershaw and Scoffin (1967)
Early diagenetic authigenic quartz	8a, f	Quartz with inclusions of sulfates, dolomites, calcites, and Na-rich liquids (EDAX, X-ray fluorescence analysis)	Idiomorphic crystals commonly pseudomorphic after anhydrite	10 – 50 μm	Early diagenetic, prior to lithification	Grimm (1962)
Pyrite I		FeS ₂	Framboidal aggregates	100 – 120 μm	Early diagenetic, linked with organic rich sediments presumably influenced by sulfur bacteria	Fabricius (1961)
Pyrite II		FeS ₂	Idiomorphic crystals	80 – 210 μm	Burial, may be linked to the migration of hydrocarbons	

6 Cements

The cement types from both the diapir reefs and the fault block reef platform are listed in Table 1 and some are discussed below.

6.1 Bladed Scalenohedral ("Dog Tooth") Cements (Figs. 4a, b, e, 7a, b)

Low-Mg scalenohedral "dog tooth" cement is the most widespread cement in the diapir reef facies. In the fault block reef facies this cement is rare. These cements appear in cavities as dripstone cements or in grainstone fabrics as meniscus cements.

According to Schneider (1977) and Pierson and Shinn (1985), scalenohedral calcites are products of freshwater diagenesis. Dog tooth (I) cements exhibit relic structures of fibrous cement neomorphic crystals. This cement was probably originally formed in the marine vadose zone (Purser 1969, Hanor 1978). Dog tooth (II) cements do not show any neomorphic characteristics. It occurs as a dripstone cement and was probably formed in the freshwater vadose zone. Dog tooth (III) cements are interpreted to be a phreatic freshwater cement (Schneider 1977).

6.2 Radial Fibrous Cements (Figs. 4d, 5d, 6b)

Two theories concern the precipitation of radial fibrous cements. According to Bechstaedt (1974), this type of cement is formed under subtidal to supratidal conditions, whereas Kendall and Tucker (1973) suggest exclusively subtidal conditions. In the diapir reefs these radial fibrous cements developed locally as a replacement of fibrous aragonitic dripstone, thus confirming the observations of Bechstaedt. That radial fibrous cements developed as a replacement of aragonitic cements is clearly suggested by the presence of relic structures, notably prismatic and spherulitic crystal aggregates. Spherulites commonly occur in the paleo-intertidal facies, whereas prismatic structures are observed in subtidal sediments. It has also been demonstrated geochemically and microscopically by Assereto and Folk (1980) that the radial fibrous cements of the Late Triassic intertidal carbonates of the southern Alps were originally aragonitic. Kendall (1985) recently investigated radial fibrous cements in Devonian reefs of western Australia and suggests that these cements are primary low or high Mg calcite formed in the marine phreatic zone. These Devonian cements show no

Fig. 4. **a** Dog tooth (I) dripstone cement – calcitic cement from the grainstones of the Villasana de Mena diapir reef (VMDRP). **b** Solution cavity of the lagoonal facies of the VMDRP and dog tooth (II) dripstone cement. **c** Equant ferroan calcite cement with enfacial junctions (1) of a stromatactis fabric in the lagoonal facies belt of the VMDRP. Internal fine-grained calcareous sediment of the stromatactis fabric (2) (crossed nicols). *Arrow* indicates upper surface. **d** Radial fibrous cement with relics of a spherulitic fabric. Intertidal belt of the VMDRP (crossed nicols). **e** dog tooth (III) cement in a large cavity of the reef flat belt of the VMDRP with *Caprina* (crossed nicols)

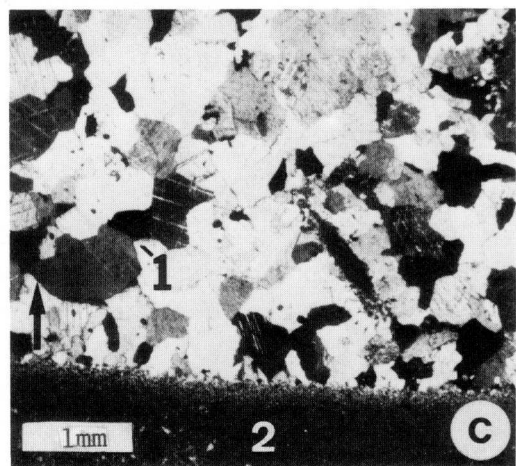
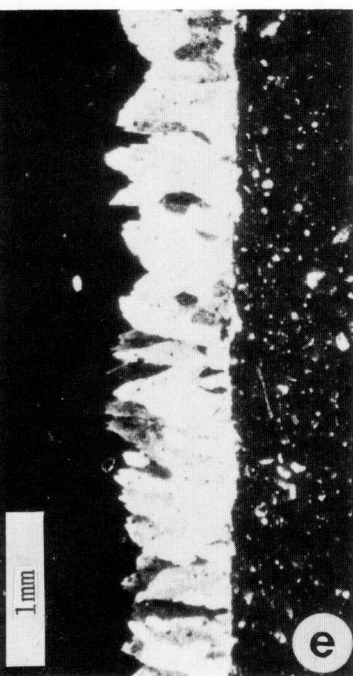
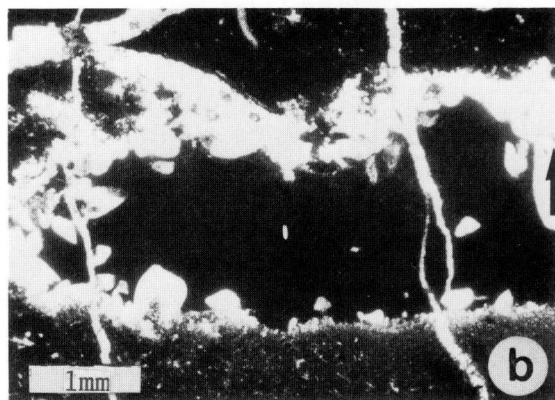
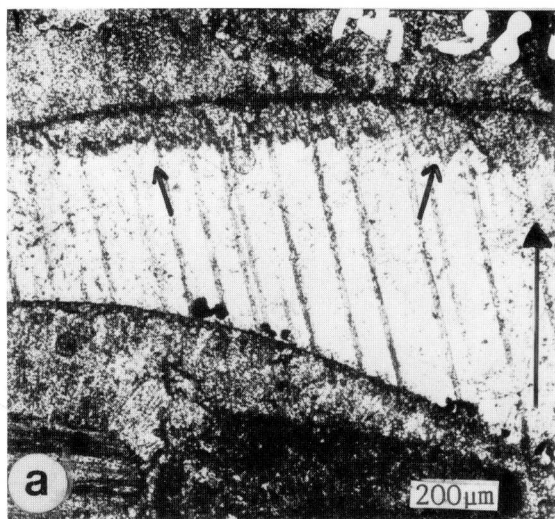


Fig. 4

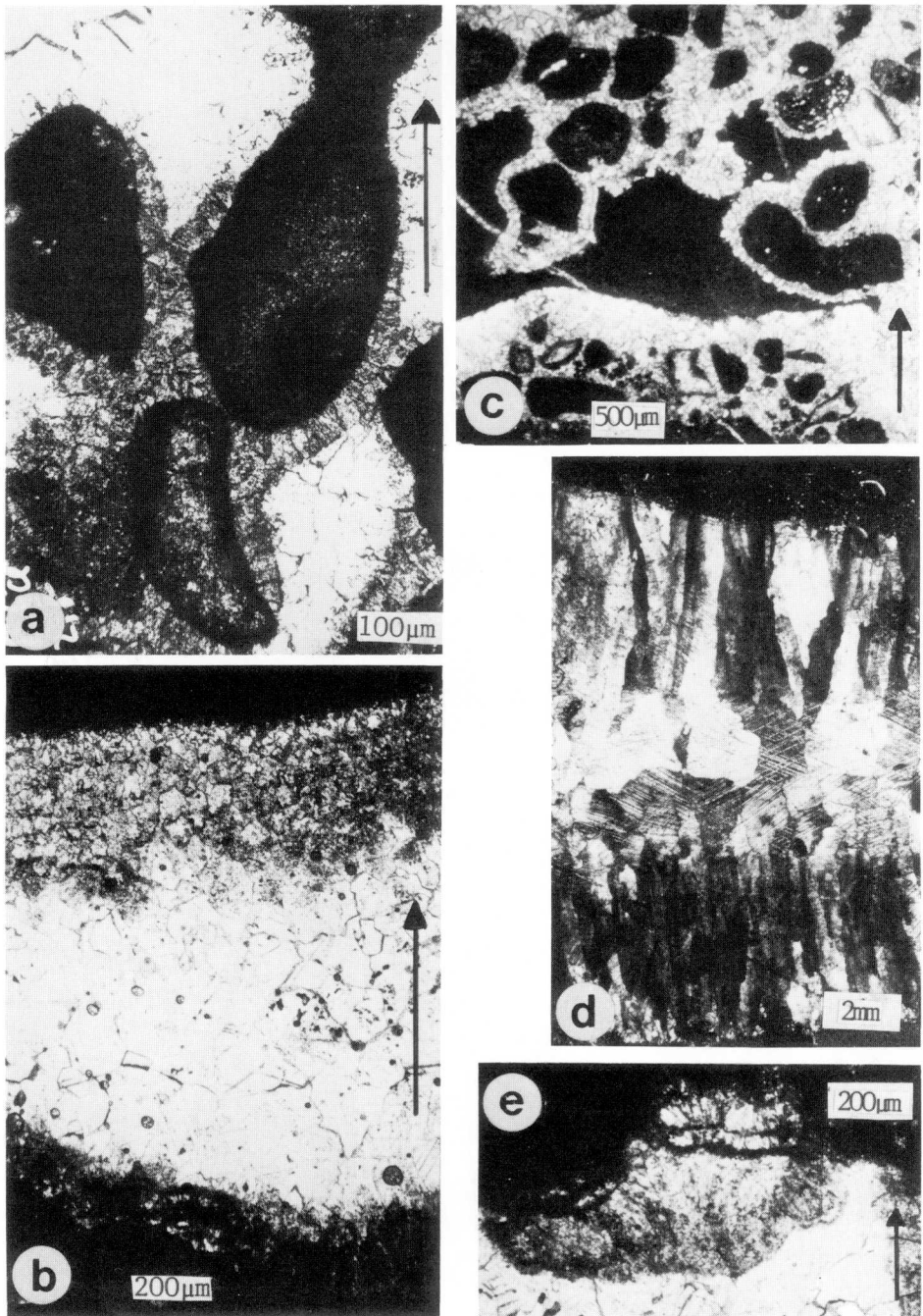


Fig. 5. **a** Meniscus cement of the reef flat belt of the VMDRP. **b** Microstalactitic and microstalagmitic dripstones from the reef core facies of the Albeniz-Eguino fault block reef platform (AEFBP). **c** Dog tooth (II) cements of the grainstones in the reef flat facies belt of the VMDRP. **d** Radial fibrous cement (1) and equant cement (2) from a sheet crack of the intertidal facies in the VMDRP (crossed nicols); **e** Fibrous dripstone cement from the reef flat facies belt of the VMDRP. Arrows indicate upper surface

relic structures while the Spanish Albian radiaxial fibrous cements do contain fibrous relic structures, suggesting different precipitation conditions.

6.3 Sulfate Cements (Fig. 7 d)

In the lagoonal facies belt of the diapir reefs, rare large cavities contain late diagenetic gypsum cements whose limpid idiomorphic crystals lack inclusions. There are two possible explanations for the formation of the gypsum cements. The sulphate may be derived from corroded pyrite which commonly occurs in the lagoon facies or it may come from the circulating diapir waters which may have been rich in dissolved sulphates.

6.4 Sulfur Cements (Fig. 8 a, b, c)

These cements are found in large cavity fillings in the lagoonal facies of the diapir reefs. The elementary sulfur originates from the reduction of anhydrite to hydrogen sulfide and the oxidation of hydrogen sulfide to sulfur by means of sulfur bacteria in the cap rock of the diapir (Feely and Kulp 1957, Ellison 1971). Both the sulfur and gypsum cements formed under deep burial conditions.

7 Authigenic Quartz

7.1 Early Diagenetic Authigenic Quartz (Fig. 8 e, f)

According to Grimm (1962), authigenic quartz forms in hypersaline conditions, an observation confirmed by Friedman and Shulka (1980). These authors describe quartz which is pseudomorphic after anhydrite and gypsum from lagoonal sediments. Bouroullec and Deloffre (1982) observe authigenic quartz pseudomorphic after anhydrite in Jurassic sabkha sediments. However, Richter (1972), Harder and Menschel (1967), and Lippmann and Schlenker (1970) demonstrate another process of authigenic quartz formation which is not related to hypersaline conditions.

The genetic relations between quartz precipitation and hypersaline conditions is evident in the Caniego Limestone of the Villasana de Mena salt diapir. However, pH is also an important factor in quartz precipitation (Grimm 1962, Friedman and Shulka 1980). Alkaline conditions ($> \text{pH } 9$) favor the precipitation of sulfates whereby quartz is dissolved, while under acidic conditions ($< \text{pH } 5$) quartz is precipitated. The formation of in-situ authigenic quartz in the Villasana de Mena diapir reef was probably influenced by both pH and hypersaline conditions. The hypersalinity was caused by the diapir waters, while the acidity probably was related to the presence of vadose freshwater. This type of quartz is not observed in the fault block reef platform.

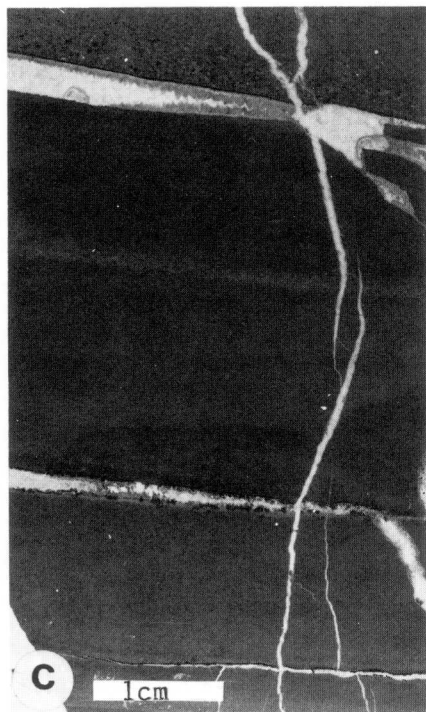
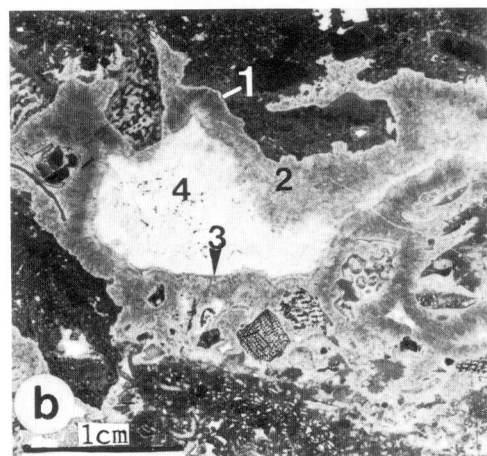
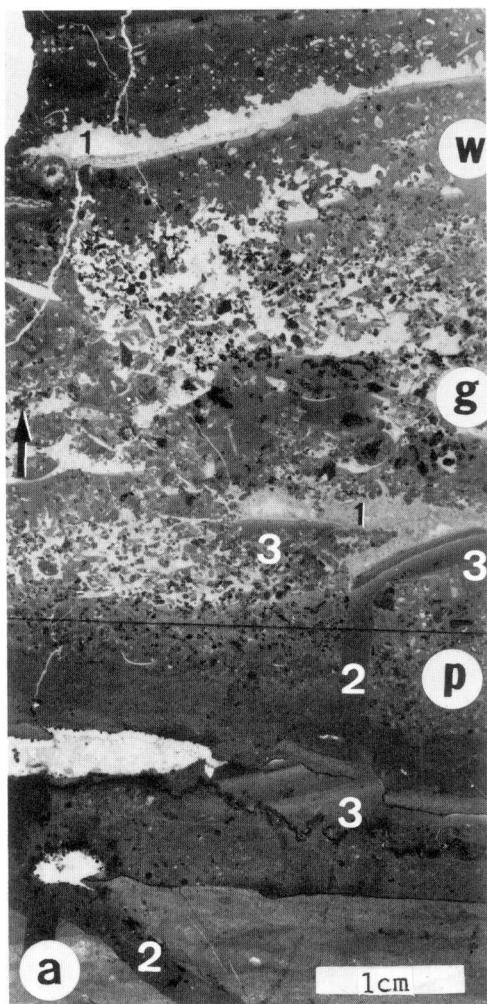


Fig. 6

7.2 Allochthonous Idiomorphic Quartz

In addition to the in-situ authigenic quartz, allochthonous idiomorphic quartz occurs in increased quantities at the base of the Caniego Limestone where a debris flow of diapir material (Keuper clays and ophites) is present (Schroeder 1980, Reitner 1982). This idiomorphic quartz is partly fractured and is identical to authigenic quartz from the Early Jurassic Carniolas Formation of this area.

8 Microstalagmitic Dripstone (Figs. 4b, 5b)

A new type of vadose cement which is reminiscent of typical cave dripstones is observed in both types of reef. According to Purser (1969), microstalactitic cement crusts (Fig. 5e) can be found in large open pores, especially in beach-rocks. In some fissures and molds microstalagmitic cements are present. This type of microcave dripstone indicates a long period during which pores remained open. There is no preferred cement type within these dripstones, but dog tooth (II) and radiaxial fibrous cements are common. The cement crystal length varies between 100 and 280 μm .

9 Microkarst

In both diapir and fault block reefs 0.5–10 cm cavities with irregular shapes cut sedimentary and biogenic structures. Such cavities are characteristic of microkarst and are morphologically distinct from stromatactis fabrics, lacking the irregularly shaped roofs and flat bottom surfaces (see Sect. 10).

10 Stromatactis (Figs. 4b, 6a)

Stromatactis-like voids occur in carbonate-rich (more than 95%) mudstones, wackestones, and bindstones of both reef types. These elongate voids measure 1–5 cm in length with a vertical width 5–10 mm. The roof of these voids is irregular while the bottom is flat and partly filled with sediment. A halo of very

Fig. 6. **a** Tempestite in lagoonal facies of the VMDRP. The tempestite contains a basal packstone unit (*p*), a central grainstone unit (*g*), and an upper wackestone unit (*w*). 1 Stromatactis fabric; 2 syndepositionary fissures with multiple micrite fillings; 3 internal sediment of the stromatactis fabric; 3' internal sediment of the stromatactis fabric rotated during a probable collapse event. **b** Large cavity in the reef core of the AEFBP. 1 Short fibrous marine cement; 2 brownish radiaxial fibrous cement; 3 vadose silt; 4 late diagenetic nonferroan calcite cement. **c** Intertidal mudstone with sheet and prism cracks filled by dripstone cements from the VMDRP. **d** Hard-ground of the basin and slope belt of the VMDRP. 1 Forereef debris (packstone); 2 phosphorite layer; 3 pyrite layer; 4 hard-ground surface with encrusting organisms; 5 pelagic mudstone. Arrows indicate upper surface

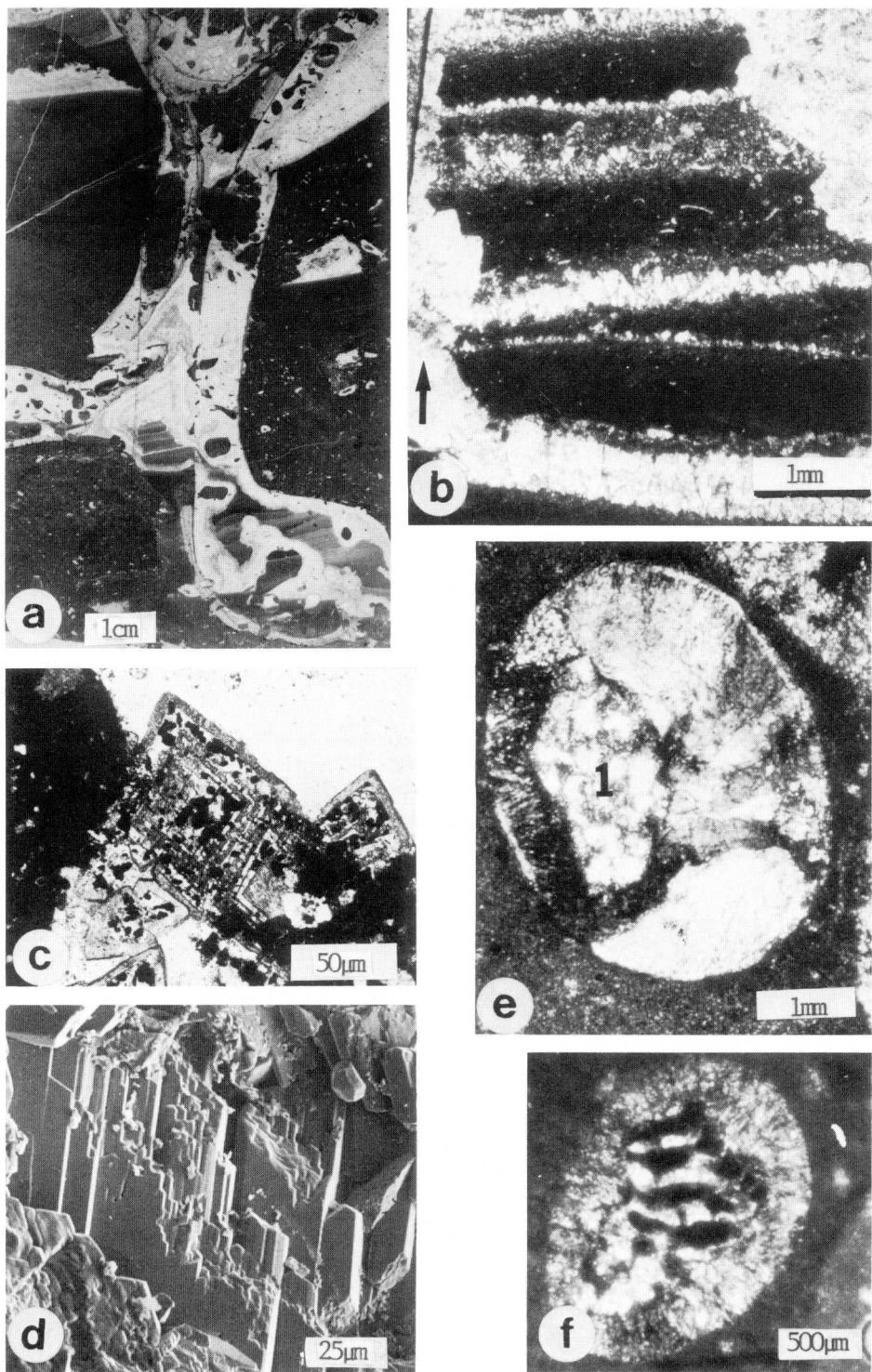


Fig. 7

dense micrite surrounds the stromatactis voids, which is in sharp contrast to the less dense micrite of the matrix rock. The grain size of both types of micrite is similar (0.5–1 μm , SEM).

These stromatactis voids presumably are the product of a very early compaction of the micritic sediment (Heckel 1972, Bechsteadt 1974). Tsien (1985), on the other hand, believes that stromatactis fabrics are biogenic in nature, as described from the type locality at St. Remi in Belgium. The origin and nature of stromatactis is unclear and Tsien gives an overview of the problem. The formation of stromatactis fabrics may well be due to a combination of both physical and biogenic processes. In the Albian reef complexes, no regularity of structures or ecological zonation is observed and the sizes of the voids are not compatible with the size of organisms such as sponges, corals, etc.

11 Interpretation of the Hard-Grounds and Stromatolitic Crusts of the Basin and Slope Belt of the Diapir Reefs (Fig. 6d)

The formation of hard-grounds and stromatolitic crusts occurred contemporaneously with sedimentation. The crusts are colonized with encrusting foraminifera, such as *Placopsilina* and *Coscinophragma*. Further evidence for syndimentary formation is the presence of hard-ground clasts in the tempestites of the lagoon facies. The hard-grounds are cut by fine pyritized strings resembling fungi mycels, suggesting participation of fungi and bacteria in the formation of the stromatolitic crusts.

The presence of phosphatic crusts (apatite) may be explained by upwelling along the diapir slope. The same process also may be responsible for reduced sedimentation rates in this area favoring the establishment of reefs. This particular hydrodynamic situation was the consequence of a change in the tectonic patterns during the Late Albian (Vraconian) (Reitner 1985). Cool waters from the deeper parts of the Bay of Biscay may have found their way into the Vasco-Cantabrian Basin and caused upwelling around the tectonic highs and diapirs. This change in hydrodynamic situation during the Late Albian resulted in the disappearance of Albian corallgal reefs, which were partly replaced by crinoid/algae bioherms (Reitner 1985).

←

Fig. 7. **a** Diagenetically altered rudists which are now filled with multiple generations of micrite and dog tooth (III) cements. Lagoon facies with *Polyconites* in the VMDRP. **b** Details of **a** illustrating the laminar fill of alternating micrite and cement. *Arrow* indicates upper surface. **c** Zoned sparry dolomite of the intertidal facies belt of the VMDRP. Gray zones are Fe-rich. **d** SEM photo of gypsum cement from the lagoon facies of the VMDRP. **e** Ooid from the Murguía diapir reef platform (MDRP) showing neomorphic calcite (crossed nicols). *l* Bioclast. **f** Radial fibrous ooid from the MDRP

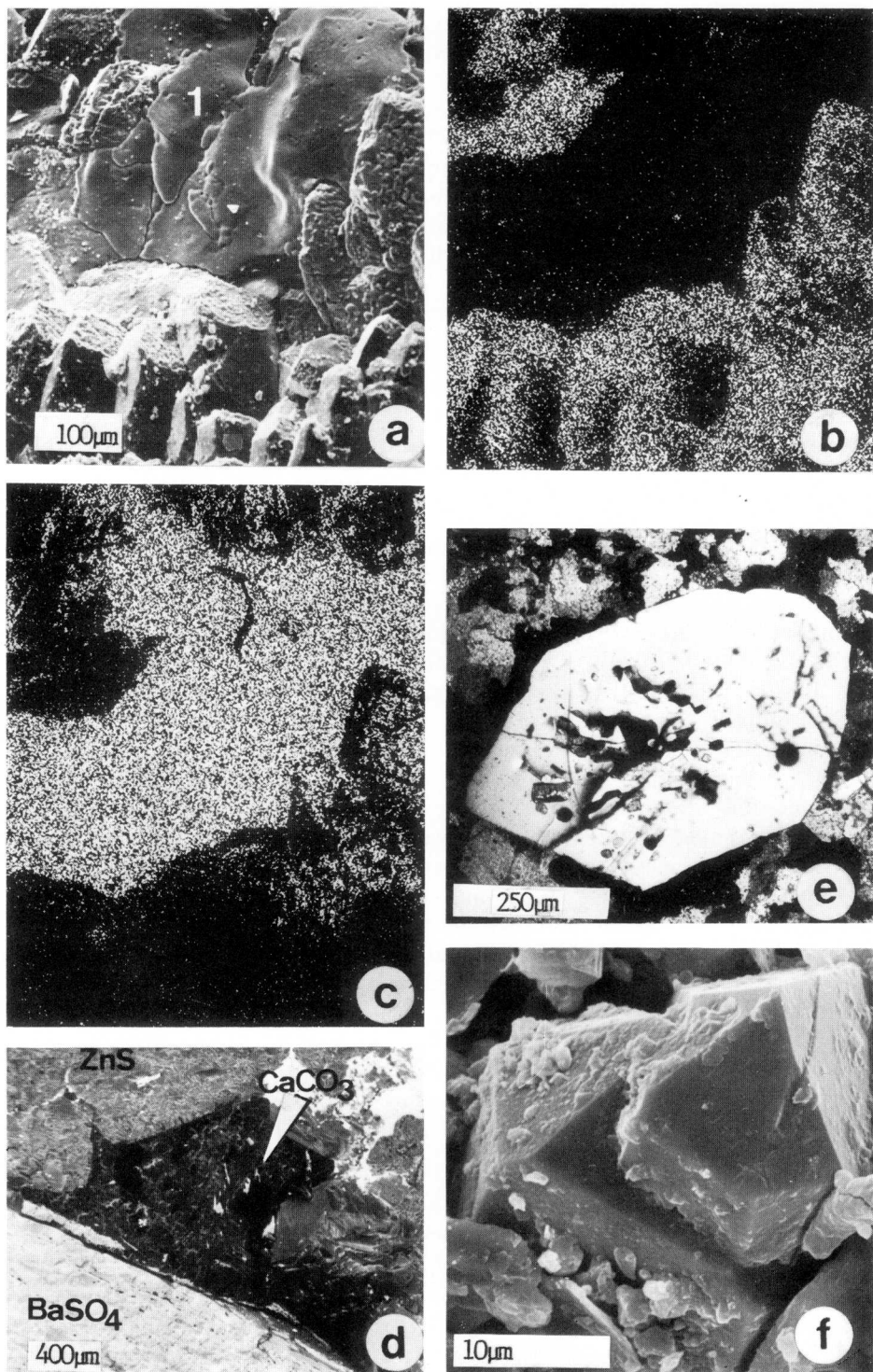


Fig. 8

12 Comparison of the Two Reefs Types (Table 2)

In the reef atoll of the Villasana de Mena diapir there occur certain cement types which are not found or are rare in the Albeniz-Eguino fault block reef. These include scalenohedral cements, certain fibrous cements, sulfur cements, gypsum cements, dolomite, and ankerite. Conversely, marine cements are rare in the diapir reef and common in the fault block reef.

Scalenohedral low Mg-calcite cements are found in molds, microkarst cavities, and primary voids as first generation cement in the diapir reefs. All described types of scalenohedrals occur; dog tooth (II) and (III) are common while dog tooth (I) is rare. The abundant occurrence of dog tooth (II) as dripstone cements within the molds and microkarst cavities indicates freshwater vadose conditions. Dripstone formation in a marine vadose environment is observed in only a few cases (dog tooth I). Within the *Polyconites* facies of the diapir reef atoll scalenohedral cements also are present in large vugs as multiple isopachous cements (dog tooth III), where cements and sediment fills alternate with the latter consisting of graded packstone, mudstones with ostracods, and calcareous silt ("vadose silt"). According to Schneider (1977) and Pierson and Shinn (1985), all scalenohedral cements are formed under meteoric conditions. Closely linked with these freshwater cements is extreme aragonite dissolution, mold formation, and microkarst, which is present in all the facies of the diapir reef atolls. Scalenohedral cements are rare in the fault block reef; they are present as neomorphic cement only in the reef flat facies.

Early marine fibrous cements are very rarely observed in the diapir reef atolls but occur infrequently in the basin and slope and reef flat facies. Radial fibrous cements commonly follow the scalenohedral cements as the next cement generation in the diapir reefs.

Certain burial cements of the diapir reef atolls appear to be closely related to the circulating diapir waters of the diapir body, these include the sulfur and gypsum cements, dolomite, and ankerite. Sulfur and gypsum cements are found in cavities in the lagoonal facies of the diapir reefs. Gypsum cement is found in the fault block reef associated only with corroded pyrite. The presence of sulfide ores in the Murguía diapir reef also tends to confirm the unique diagenetic influence of diapirs on reef carbonates since these phenomena are not observed in the fault block reef.

Dolomites and ankerites, the last cementation phase, destroy former cements and crystallize in tectonic fissures. The cement filling of the large fissures (width of several decimeters) are dark drusy and fibrous calcite and are presumably the youngest of the late cements, since the fissure systems show a radial pattern linked to the last diapir collapse in the Late Tertiary.

←
Fig. 8. **a** Diagenetic sulfur cement in a large dissolution cavity of the lagoonal mudstone facies of the VMDRP (1) (SEM photo). **b** Calcium distribution pattern from the sulfur cement of **a**; scale as in **a**. **c** Sulfur distribution pattern from the sulfur cement of **a** (1000 counts s^{-1} ; 20 kV); scale in **a**. **d** Ore paragenesis in a fissure of the MDRP (SEM photo). **e** Large early diagenetic authigenic quartz with Na-rich inclusions in the lagoonal facies of the VMDRP (crossed nicols). **f** Authigenic quartz from the lagoonal mudstone of the VMDRP (SEM photo)

Table 2. The differences between fault block reefs and diapir reefs

Fault block reefs	Diapir reefs
<i>Reef Structure</i>	
Island platforms with isolated reefs, ca. 15 × 20 km	Atolls and small pinnacle ca. 5 × 5 km
<i>Organism diversity of selected groups</i>	
Corals: 36 species	Corals: 5 species
Sponges: 11 species	Sponges: 8 species
Mg-calcite algae: 6 species	Mg-calcite algae: 4 species
Aragonite algae: 15 species	Aragonite algae: 2 species
Stromatolites: rare	Stromatolites: abundant
Molluscs: 18 species	Molluscs: 8 species
<i>Microfacies</i> (field observation, quantitative analysis of profiles)	
Micrite – sparite	Micrite – sparite
70 : 30	90 : 10
Mudstone rare	Mudstone with authigenic quartz common
<i>Geochemistry</i>	
Sr 300–1300 ppm	Sr 100–250 ppm
Mn 100–500 ppm	Mn 100–1600 ppm
Fe 100–20000 ppm	Fe 300–30000 ppm
Na 110–400 ppm	Na 60–3300 ppm
Mg 120–4000 ppm	Mg 140–5400 ppm
<i>Diagenesis</i>	
Early marine cements in all facies zones, except in the intertidal zones;	Early marine cements rare;
Neomorphism of aragonite	Meteoric cements abundant;
Calcite ooids	Early diagenetic authigenic quartz formed by hypersaline solutions;
	Late diagenetic gypsum and sulfur cements;
	Burial dolomite and ankerite;
	Multiphased sedimentation and cementation in cavities;
	Sulfide ores;
	Aragonitic ooids

The fault block reef exhibits a totally different cementation history. The abundance of marine cements, especially radial fibrous and short fibrous cements, is in direct contrast to the diapir reefs. An intense freshwater diagenesis is not observed except in the intertidal and reef core facies of the Albeníz-Eguino fault block reef platform. The cementation sequence is controlled by subsidence of the fault block. It appears, therefore, that the principle diagenetic difference between the two types of reefs concerns the timing of the freshwater diagenesis which is related to differing fault block and diapir movements.

13 Discussion and Conclusions

The key difference between diapir reef atolls and fault block reef platform diagenesis appears to be the early introduction of meteoric water into the diapir reef

complex. This is demonstrated by the presence of certain non-marine cements, dissolution of fossils, microkarst, extremely low Sr (100–250 ppm), and Mg values (500–1600 ppm) (results from bulk analyses of limestones in the diapirs). Also interesting is a comparison of high-Mg calcite sponges (*Acanthochaetetes*) between the two reef types. The sponges of the fault block reef contain more than twice the amount of Mg than the diapir reef sponges. Within the Villasana de Mena diapir reef geochemical anomalies were also noted for the trace elements Na, Fe, and Mn. The Na values of up to 3300 ppm, the Fe content of up to 30000 ppm, and the Mn values of up to 1500 ppm were measured in the soluble portion of the limestone from the reef facies. The anomalies are linked both with large amounts of reworked Keuper sediments from the diapir and with early diagenetic quartz caused by the extruding hypersaline brines associated with the syn-sedimentary collapse event of the diapir and the corroded Keuper ophites (continental tholeiites, Meschede 1985). It is evident that diapiric movement was active during reef development.

Fossil constituents also confirm both the diagenetic and the sedimentary differences between diapir and fault block reefs. In all facies within the diapir reef complex organism preservation is significantly poorer than in the fault block reef platforms. The reduction mainly affects organisms with aragonitic skeletons, the intense early meteoric diagenesis causing the selective dissolution of aragonite. Low animal diversity may also be due partly to unfavorable ecological conditions reflecting the hypersalinity in these diapir-influenced reefs.

All peculiarities of the diapir reef platform may therefore related to the movement of the diapir. Thus, meteoric diagenesis, the multiple sediment filling, and the cementation may have been conditioned by the repeated, but relatively brief, elevations of the diapir. These periodic movements brought the reef complex repeatedly into the vadose environment. Each emergence of the entire reef complex resulted in the multiple filling of the reef cavities and cementation of the sediments with a meteoric cement, as well as the death of the reef fauna. The mobility of the diapirs may have resulted from the complicated interplay of general subsidence of the Vasco-Cantabrian Basin, ascent of the diapir, sea level changes, and dissolution processes in the diapir subsequent to collapse events.

This oscillating vertical movement is not found in the Albeníz-Eguino fault block reef platform. The absence of certain cements, such as sulfur and sulfate cements, and of diapir-linked sulfur ores, as in the Murguía diapir reef, also demonstrates the lack of diapir influence in the burial conditions of the fault block reef. The geochemical data from the Albeníz-Eguino fault block reef platform exhibits high Sr values of 200–1500 ppm (mean values approx. 400 ppm), which are not observed in the diapir reef atolls.

Modern examples of diapir reef atolls can be found in the Gulf of Mexico as pinnacle reefs (West Flower Garden Bank). The faunal and floral diversity of these diapir pinnacle reefs are significantly less than in the fault block reef platforms in the Caribbean (Reitner 1982). However, the direct influence of diapiric brines and diapir material on the reef complex has not yet been observed. Ancient examples of diapir-influenced reefs outside the Vasco-Cantabrian Basin are known from the Albian of Tunisia, which exhibit typical collapse structures. Such diapir reefs are of considerable value in oil and gas exploration (Maurin 1980).

Acknowledgments. The author thanks Dr. T. Engeser and Dr. E. Gierlowski-Kordesch for assistance in translation and critical reading, and the Comision Nacional de Geología Madrid (Spain) for providing access to the field area (100/80). The field work was financed by the Deutsche Forschungsgemeinschaft (SFB 53, F20).

The studies were carried out in the Geological Institute of the University of Tübingen and in the Institute of Paleontology of the Free University of Berlin. Some SEM analysis were carried out at the Bundesanstalt für Materialprüfung (BAM) in Berlin.

References

- Assereto R, Folk RL (1980) Diagenetic fabrics of aragonite, calcite, and dolomite in an ancient peritidal-spirographen environment: Triassic calcareo rosso Lombardia, Italy. *J Sediment Petrol* 50:371–394
- Bechstaedt T (1974) Sind Stromatactis und radiaxial-fibroses Calcit Faziesindikatoren? *N Jahrb Geol Palaeontol Monatsh* 1974:643–663
- Blank R (1983) Stratigraphie und Entwicklung der Oberkreide im Westteil des Diapir von Villasana de Mena (Prov. Burgos, Norspanien). Diplom Thesis, Eberhard-Karls Univ Tübingen
- Bouroulec J, Deloffre R (1982) Les Paléobasins du Jurassique Terminal en Aquitaine (SW France). *Bull Cent Rech Explor Prod Elf-Aquitaine* 6:227–255
- Brinkmann R, Loegters H, Pflug R, von Stackelberg U, Hempel PM, Kind HD (1967) Diapir-Tektonik und Stratigraphie im Vorland der spanischen Westpyrenäen. *Beih Geol Jahrb* 66:1–183
- Ellison SP (1971) Sulfur in Texas. *Bur Econ Geol* 2:1–48
- Fabricius FH (1961) Die Strukturen der „Rogenpyrite“ (Koessener Schichten, Raet) als Beitrag zum Problem der „Vererzten Bakterien“. *Geol Rundsch* 51:311–319
- Feely HW, Kulp KL (1957) Origin of Gulf Coast Salt Dome Sulphur Deposits. *Am Assoc Petrol Geol Bull* 41:1802–1853
- Fischer AG (1964) The Lofer cyclothems of the Alpine Triassic. *Bull Kansas Geol Surv* 169:107–149
- Folk RL, Land LS (1975) Mg/Ca ratio and salinity: two controls over crystallization of dolomite. *Am Assoc Petrol Geol Bull* 59:60–68
- Friedman GM, Shulka V (1980) Significance of authigenic quartz euhedra after sulphates: example from the Lockport Formation (Middle Silurian) of New York. *J Sediment Petrol* 50:1299–1304
- Grimm WD (1962) Idiomorphe Quarze als Leitminerale für salinare Fazies. *Erdöl Kohle Erdgas Petrochem* 11:880–887
- Hanor JS (1978) Precipitation of beachrock cements: mixing of marine and meteoric waters versus carbon dioxide degassing. *J Sediment Petrol* 48:489–501
- Harder H, Flemhig W (1967) Bildung von Quarz aus verdünnten Lösungen bei niedrigen Temperaturen. *Naturwissenschaften* 54:140
- Harder H, Menschel G (1967) Quarzbildung am Meeresboden. *Naturwissenschaften* 54:561
- Heckel PH (1972) Possible inorganic origin for stromatactis in calcilitite mounds in the Tully Limestone, Devonian of New York. *J Sediment Petrol* 42:7–18
- Kendall AC (1985) Radiaxial fibrous calcite: a reappraisal. In: Schneidermann N, Harris PM (eds) Carbonate cements. *Soc Econ Paleontol Miner Spec Publ* 36:59–77
- Kendall AC, Tucker P (1973) Radiaxial fibrous calcite: a replacement after acicular carbonate. *Sedimentology* 20:365–389
- Lietz J (1951) Sulfidische Klüfterze im Deckgebirge des Salzstockes Reitbrook. *Mitt Geol Staatsinst Hamburg* 20:110–118
- Lippmann F (1973) *Sedimentary Carbonate Minerals*. Springer, Berlin Heidelberg New York Tokyo
- Lippmann F, Schlenker B (1970) Mineralogische Untersuchungen am Oberen Muschelkalk von Haigerloch (Hohenzollern). *N Jahrb Miner Abh* 113:68–90
- Longman MW (1980) Carbonate diagenesis textures from nearshore diagenetic environments. *Am Assoc Petrol Geol Bull* 64:461–487
- Lotze F (1953) Salzdiapirismus im nördlichen Spanien. *Z Dtsch Geol Ges* 105:814–822
- Mattes BW, Mountjoy EW (1980) Burial dolomitisation of the Upper Devonian Miette Buildup, Jasper National Park, Alberta. *Soc Econ Paleontol Miner Spec Publ* 28:259–297

- Maurin AF (1980) Halocinèse et sédimentologie – un thème de réflexion. *Trav Lab Geol Hist Paleontol* 11:18 – 19
- Meschede M (1985) The geochemical character of volcanic rocks of the Basco-Cantabrian Basin, northeastern Spain. *N Jahrb Geol Palaeontol Monatsh* 1985:115 – 128
- Neugebauer J, Ruhmann G (1978) Experimentelle Karbonatzementation: Syntaxialer Calcit auf Echinodermen. *N Jahrb Geol Palaeontol Monatsh* 1978:545 – 555
- Oldershaw AE, Scoffin TP (1967) The source of ferroan and non-ferroan calcite cements in the Halkin and Wendlock Limestones. *Geol J* 5:309 – 320
- Pierson BJ, Shinn EA (1985) Cement distribution and carbonate mineral stabilization in Pleistocene limestones of Hogsty Reef, Bahamas. In: Schneidermann N, Harris PM (eds) *Carbonate Cements. Soc Econ Paleontol Miner Spec Publ* 36:153 – 168
- Purser BH (1969) Syndimentary marine lithification of Middle Jurassic limestones in the Paris Basin. *Sedimentology* 12:205 – 230
- Ramirez del Pozo J (1971) Bioestratigrafía y microfácies del Jurásico y Cretácico del Norte de España. *Mem Inst Geol Miner España* 78:1 – 357
- Reitner J (1980) Fazies, Bau und Stratigraphie der Riffkalk-Zone (Mittel-Oberalb) im Raum Araya-Alsasua (Prov. Alava/Navarra, Nordspanien) und ein Vergleich mit dem Caniego-Riffkalk (Oberalb) bei Villasana de Mena (Prov. Burgos, Nordspanien). *Diplom Thesis, Eberhard-Karls Univ, Tübingen*
- Reitner J (1982) Die Entwicklung von Inselplattform und Diapir-Atollen im Alb des Basko-Kantabrikums (Nordspanien). *N Jahrb Geol Palaeontol Abh* 165:87 – 101
- Reitner J (1985) Mikrofazielle, palökologische und palaeontologische Analyse ausgewählter Vorkommen flachmariner Karbonate im Basko-Kantabrischen Strike-Slip Fault-Becken-System (Nordspanien) an der Wende von der Unterkreide zur Oberkreide. *Dissertation, Eberhard-Karls Univ, Tübingen*
- Richter DK (1972) Authigenic quartz preserving skeletal material. *Sedimentology* 19:211 – 218
- Sandberg PA (1975) New interpretation of Great Salt Lake ooids and of ancient non-skeletal carbonate mineralogy. *Sedimentology* 22:497 – 537
- Sandberg PA (1983) An oscillating trend in Phanerozoic non-skeletal carbonate material. *Nature* 305:19 – 22
- Schneider W (1977) Diagenese devonischer Karbonatkomplexe Mitteleuropas. *Geol Jahrb* 21(D):1 – 107
- Schroeder R (1980) Le calcaire de Caniego: témoin d'une montée du diapir de Valle de Mena (Prov. Burgos, Espagne) dans l'Albian supérieur. *Cuad Geol Iber* 5:221 – 225
- Schroeder R, Willems H (1983) Über einen submarinen Durchbruch des Diapirs von Villasana de Mena (Prov. Burgos, N-Spanien) an der Wende Unter-/Oberkreide. *N Jahrb Geol Palaeontol Abh* 166:65 – 85
- Stackelberg von U (1967) Der Diapir von Murguía. *Beih Geol Jahrb* 66:63 – 94
- Tsien MM (1985) Origin of stromatolites – a replacement of colonial microbial accretions. In: Toomey DF, Nitecki MH (eds) *Paleoalgology*. Springer, Berlin Heidelberg New York, pp 274 – 298